Supporting Information

Work Function Dependence of Vibrational Relaxation Probabilities: NO($v = 2$) Scattering from Ultra-Thin Metallic Films of Ag/Au(111)

Christoph Steinsiek *[1], *Pranav R. Shirhatti* [1,2(a)], *Jan Geweke* [1,2,3], *Christof Bartels* [1,5], *Alec M. Wodtke* [1,2,3,4].

[1]Institute for Physical Chemistry, Georg-August University of Göttingen, Tammannstraße 6, 37077 Göttingen, Germany.

[2]Department of Dynamics at Surfaces, Max Planck Institute for Biophysical Chemistry, Am Faßberg 11, 37077 Göttingen, Germany.

[3]Max-Planck-EPFL Center for Molecular Nanoscience and Technology, Institute of Chemical Science and Engineering (ISIC), Station 6, École Polytechnique Fédérale de Lausanne (EPFL), CH-1015 Lausanne, Switzerland.

[4]International Center for Advanced Studies of Energy Conversion, Georg-August University of Göttingen, Tammannstraße 6, 37077 Göttingen, Germany,

[5]Physikalisches Institut, Universität Freiburg, Hermann-Herder-Straße 3, 79104 Freiburg, Germany

[(a)] Present address: Tata Institute of Fundamental Research, 36/P, Gopanapally Village, Serilingampally Mandal, Ranga Reddy District, Hyderabad 500107, India

I.QCM calibration and sample characterization

The scattering experiments of the present work were performed with a Au(111) single crystal which was coated with silver with a thickness gradient along one axis. This required a) a calibration of the quartz crystal microbalance (QCM) to monitor the film growth and b) a method to obtain the film thickness at a certain crystal position. Both procedures will be described in the following section.

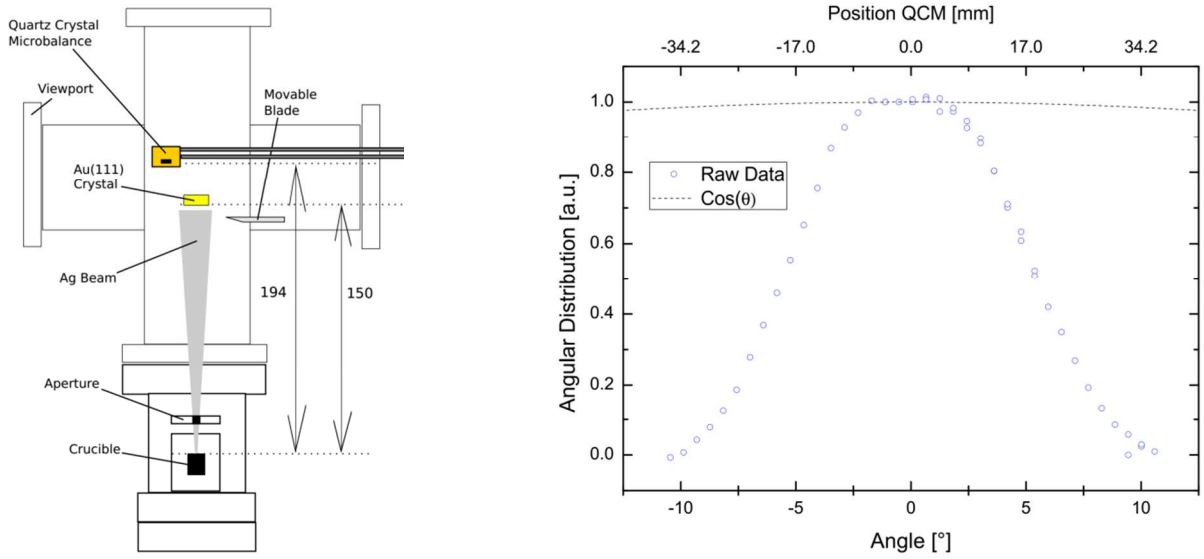

Fig. S1.: Left panel: Sketch of the evaporation stage. Double arrows display distances of the evaporator to the substrate and the QCM. Right panel: Angular distribution of the silver beam measured by moving the QCM along one axis.

On the left panel of Fig. S1, the evaporation stage during a homogenous deposition process (no use of the movable blade) is sketched. The angular distribution of the silver beam was obtained with the QCM (right panel). The Au(111) and the QCM are at different distances to the crucible, therefore the readout at the QCM does not reflect the correct thickness deposited on the crystal. For a calibration, geometrical distances and the angular distribution were employed in a simple model of a point source and it was estimated that a value ~1.3 Å as determined from the QCM readout would correspond to the deposition of 1 ML Ag/Au (2.4 Å) on the Au(111) crystal.

The final calibration value was obtained in an experimental procedure using Auger Electron Spectroscopy (AES). Starting with a clean Au(111), a small amount of silver was (homogeneously) deposited on the surface and an AES spectrum was acquired. Those steps were repeated sequentially and the Auger peak to peak heights (APPHs) of Au and Ag were plotted against the film thickness as recorded by the QCM. Because of the layer-by-layer growth of Ag/Au, those signals are expected to exhibit a linear trend during the formation of a monolayer and a slope discontinuity occurs when each monolayer is completed (Ref: Tokutaka, H.; Nishimori, K.; Takashima, K., A Quantitative AES Method for the Study of a Monolayer Overgrowth of Thin Film, *Surf. Sci.* **1979**, 86, 54-61) . Considering the previous geometric estimation, it was aimed to measure >10 points during the buildup of one monolayer. The normalized APPHs are depicted in Fig. S2, left panel.

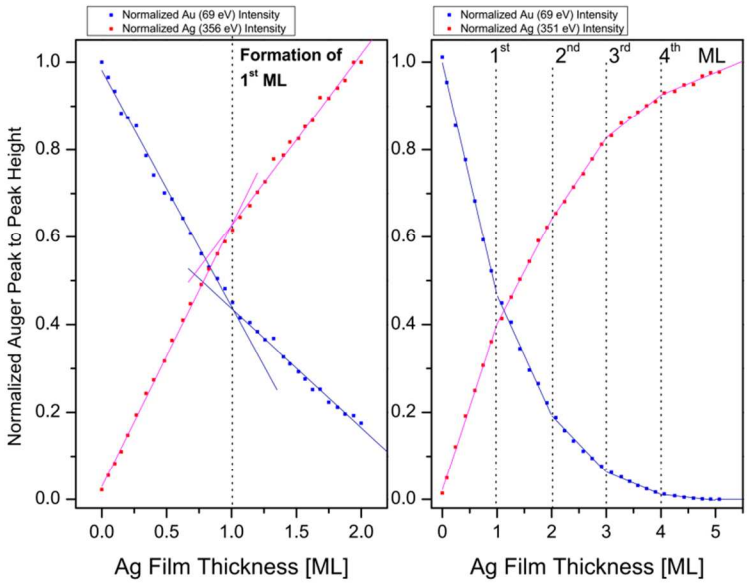

Fig. S2.: Calibration of the QCM: the normalized APPH of Au and Ag is plotted against the (calibrated) QCM readout. After cleaning and annealing of the Au(111) surface, Ag deposition and acquisition of Auger spectra were performed in a subsequent manner. Left panel: Measurement at small step size (>10 points per ML). Linear behavior during the buildup of a single layer is observed with a breakpoint after completion of a full layer which was determined by fitting a model consisting of two straight lines. Right panel: A model of five subsequent straight lines with the previously determined calibration value is fitted to each data set for visualization of the kinks after completion of the first four monolayers of Ag/Au(111).

A model consisting of two straight lines was fitted onto the acquired data and a minimum of the root mean square error was numerically obtained for both datasets of Au and Ag. The result that a QCM readout of 1.2 Å corresponds to a deposition of 1 ML Ag/Au at the crystal was used as the final calibration value. Estimating an error of 0.1 Å, that value is in good agreement with the previous estimation.

Figure S2 (right panel) shows the data of a similar measurement with a lower point density but greater thickness range during the growth of the first four monolayers. When fitting a model consisting of a sequence of straight lines using the calibration value, distinct slope discontinuities after the formation of integer numbers of layers are clearly recognized.

The present data shows that both elements Ag and Au can be detected by AES up to a film thickness of ~4 ML Ag/Au. Within this thickness range, the Ag/Au ratio is obtained for different film thicknesses which provides a tool to determine the film thickness at any position on the sample even after the deposition process.

During the calibration procedure, the Au(111) crystal was coated uniformly on the crystal. However, to perform film thickness-dependent scattering experiments efficiently, it is advantageous to prepare a sample that provides not only a single but several different film thicknesses. This was achieved in the experiment by employing a movable blade (sketched in Fig. S1, left panel) which was connected to a stepper motor. Partially blocking the silver beam during deposition, we prepared samples with wedge-like thickness-gradients of Ag/Au along one axis.

Scanning along this axis with AES, a position dependent film thickness can be measured. As an example, Fig. S3 shows the thickness profile measured at different positions on the crystal. During the deposition, it was intended to grow a sample with a small region of clean Au(111) and a linear wedge with maximum thickness of 2.4 ML as controlled by the QCM. The AES measurements nicely confirm these characteristics.

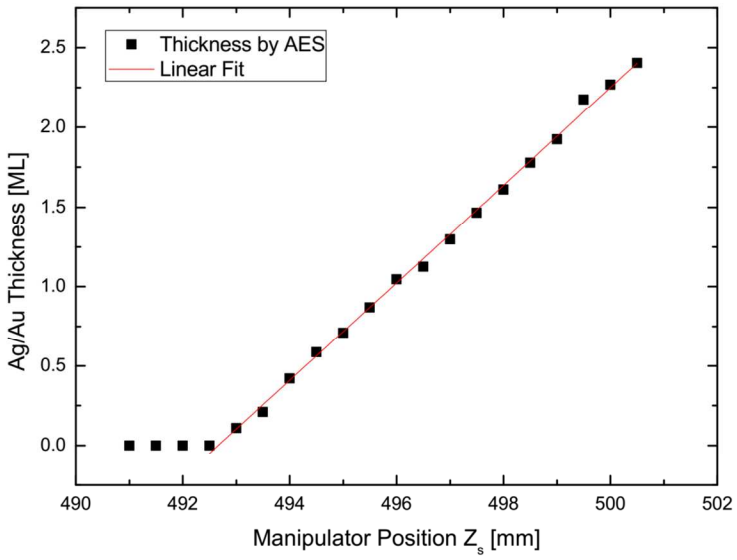

Fig. S3: Film thickness against the position of the Au(111) crystal for a wedge of 0-2.4 ML Ag/Au. Using AES, film thickness was measured along surface by moving the z axis of the manipulator in 0.5 mm steps. Beside a few positions of a clean Au(111) (0-3mm), the film thickness increases in an almost perfect linear manner.

During the growth of wedge samples with a thickness maximum above 4 ML, it was assumed that such a sample will exhibit a linear thickness increase along the axis as well. For such cases, the thickness assignment was performed in a slightly different manner. Crystal positions with thicknesses below 4 ML were assigned by the AES method. An additional data points of the wedge's maximum thickness is determined by the QCM. With the assumption of a linear thickness gradient, points in between have been interpolated from the available data.

Because the sample is of limited sample size, the estimated error depends strongly on the thickness gradient. For the sample of a maximum thickness of 4 ML, the thickness increase is about 0.6 ML per mm. By assuming a positioning error of 0.25 mm, the error of the thickness assignment is estimated to be about 0.2 ML. For the wedge of 10 ML maximum thickness with a gradient of 1.5 ML/mm, we estimate 0.4 ML.

2. Extracting absolute scattering probabilities

a) Extending the acquisition procedure to compare different surfaces

In general, the evaluation of vibrational relaxation probabilities follows the method as reported previously (Cooper, R.; Li, Z.; Golibrzuch, K.; Bartels, C.; Rahinov, I.; Auerbach, D. J.; Wodtke, A. M., On the Determination of Absolute Vibrational Excitation Probabilities in Molecule-Surface Scattering: Case Study of NO on Au(111), *J Chem Phys* **2012**, *137*, 064705). NO is prepared in an initial vibrational state $v = 2$. After scattering from the surface, molecules can be found in the same ($v = 2$) or a lower ($v = 1,0$) vibrational state. Excitation to higher states ($v = 3$, 4,…) is negligible for a surface at room temperature. The probability of NO($v_i = 2$) to relax selectively into the final state $v_f = \mathrm{x}$ is defined by the ratio of scattered molecules $N_{v=x}$ to the sum of all scattered molecules $\sum_i N_{v=i}$.

$$P_{v=2\rightarrow x} = \frac{N_{v=x}}{\sum_i N_{v=i}} \qquad \text{(SI 2.1)}$$

Quantitative information about the number of molecules $N_{v=x}$ in a vibrational state can be obtained from the integrated spectral intensity $\int S_v(\lambda)d\lambda$, where the spectrum is recorded over a specific vibrational band. Such measurements are strongly affected by fluctuations of the laser power which was continuously monitored allowing a point-to-point correction. Furthermore, the integrated spectral intensity is influenced by several factors like the angular distribution $\Theta_v(\theta)$, the arrival time distribution $\Delta(\tau_v)$ and the Franck-Condon factors FCF_{v} of the corresponding vibrational band. To minimize corrections, the detector gain Γ_v determined by the voltage of the MCP detector was kept constant. Because acquisition via REMPI is a density-dependent detection technique, density-to-flux conversion is carried out by multiplying with the scattered

mean velocity $\langle s_v \rangle$. All corrections included, the intensity of different vibrational states can be quantitatively compared:

$$N_v \propto \langle s_v \rangle \cdot \Theta_v \cdot \Delta(\tau_v) \cdot FCF_v^{-1} \cdot \Gamma_v \cdot \int S_v(\lambda) d\lambda \qquad \text{(SI 2.2)}$$

As in a previous study (Huang, Y.; Wodtke, A. M.; Hou, H.; Rettner, C. T.; Auerbach, D. J., Observation of Vibrational Excitation and Deexcitation for NO(v=2) Scattering from Au(111): Evidence for Electron-Hole-Pair Mediated Energy Transfer, *Physical Review Letters* **2000**, *84*, 2985-2988), the absolute relaxation probability of NO(v = 2) from Au(111) has been determined assuming that relaxation into v = 0 is negligible which seems justified in the light of only low two quanta relaxation for NO(v = 3) (see Fig. 10 in Golibrzuch, K.; Shirhatti, P. R.; Rahinov, I.; Kandratsenka, A.; Auerbach, D. J.; Wodtke, A. M.; Bartels, C., The Importance of Accurate Adiabatic Interaction Potentials for the Correct Description of Electronically Nonadiabatic Vibrational Energy Transfer: A Combined Experimental and Theoretical Study of NO(v = 3) Collisions with a Au(111) Surface. *J Chem Phys* **2014**, *140*, 044701).

For the comparison of relaxation at a Ag/Au(111) surface with Ag film thickness *T* monolayers to a clean reference surface Au(111), a relative relaxation probability $P_{rel,v=2\rightarrow x}$ is introduced. In combination with equation (SI 2.1), this measure can be expressed by comparing the number of molecules scattered from a film thickness *T* and from the reference surface:

$$P_{rel,v=2\rightarrow x}(T) = \frac{P_{v=2\rightarrow x}(T)}{P_{v=2\rightarrow x}(0)} = \frac{N_{v=x}(T)}{N_{v=x}(0)} \qquad \text{(SI 2.3)}$$

For a single vibrational state and constant detector gain Γ_v, N_v can be substituted according to equation (SI 2.2).

$$P_{rel,v=2\rightarrow x}(T) = \frac{\langle s_{v=x}\rangle(T)}{\langle s_{v=x}\rangle(0)} \cdot \frac{\Theta_{v=x}(T)}{\Theta_{v=x}(0)} \cdot \frac{\Delta(\tau_{v=x},T)}{\Delta(\tau_{v=x},0)} \cdot \frac{\int S_{v=x}(\lambda,T)d\lambda}{\int S_{v=x}(\lambda,0)d\lambda} \quad \text{(SI 2.4)}$$

Introducing a few abbreviations for the relative signal and the three correction factors

$$SIG_{rel,x} = \frac{\int S_{v=x}(\lambda,T)d\lambda}{S_{v=x}(\lambda,0)d\lambda},\ CF_{Ang,x}=\frac{\Theta_{v=x}(T)}{\Theta_{v=x}(0)},\ CF_{TOF,x}=\frac{\Delta(\tau_{v=x},T)}{\Delta(\tau_{v=x},0)},\ CF_{DTF,x}=\frac{\langle s_{v=x}\rangle(T)}{\langle s_{v=x}\rangle(0)} \quad \text{(SI 2.5)}$$

in accordance with (SI 2.3), the absolute scattering probability of a diatomic molecule scattered from a Ag/Au surface can be obtained as

$$P_{v=2\rightarrow x}(T\ \text{ML}) = P_{v=2\rightarrow x}(\square\text{u}) \cdot SIG_{rel,x} \cdot CF_{Ang,x} \cdot CF_{TOF,x} \cdot CF_{DTF,x} \quad \text{(S I2.6)}$$

which allows to obtain the absolute relaxation probabilities of the observed final states v = 2,1.

Relaxation into v = 0 cannot be directly measured but the simultaneous signal decrease observed for NO(v = 2), with NO(v = 1) remaining approximately constant, is interpreted as an increase of relaxation into v = 0. The relaxation into this channel is estimated as:

$$P_{v=2\rightarrow 0}(T) = 1 - P_{v=2\rightarrow 2}(T) - P_{v=2\rightarrow 1}(T) \quad \text{(SI 2.7)}$$

b) Comparing two acquisition strategies

An immediate impression about the relaxation of NO(v = 2) after scattering from a certain surface can be obtained when comparing raw state-selective REMPI data. Fig. S4 (top panel) shows raw spectra of the NO($v = 2 \rightarrow 2$) channel scattered from Au(111) and a thickness of 5 ML Ag/Au(111). For this measurement, the annealed Au(111) surface was partly shadowed by the (non-moving) mask during the deposition process resulting in a crystal with one half covered by 5 ML Ag/Au and the other half consisting of clean Au(111). Apart from the different surface

positions chosen for the scattering experiments, both REMPI spectra have been acquired with the same experimental settings. At a thin film, the NO(v =2 → 2) signal is strongly decreased due to strong relaxation of NO(v = 2) into lower vibrational states.

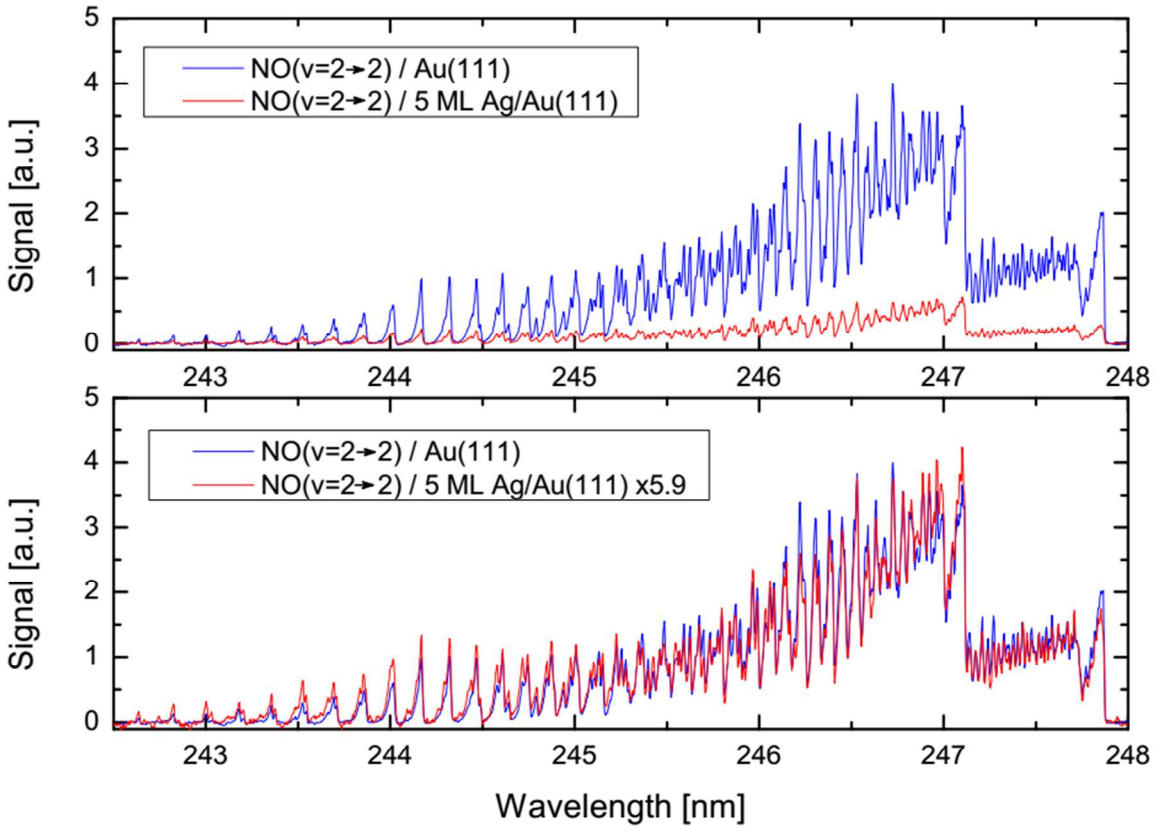

Fig. S4: Top panel: State-selective NO(v = 2→2) spectrum after scattering from surface positions with clean Au(111) (blue) and 5 ML Ag/Au(111) (red). The signal is strongly decreased from a coated surface due to increased relaxation into lower vibrational states. Bottom panel: A constant factor is used to scale the spectrum obtained from the coated surface which leads to almost perfect agreement with the spectra obtained from Au(111). We conclude the rotational distribution does not depend on the film thickness.

In the bottom panel, the spectrum after scattering from the thin film sample was scaled by a constant factor which leads to an almost perfect agreement of both acquired signals. We concluded that the rotational distribution does not significantly change when scattering is performed on Ag/Au in comparison to clean Au(111).

As a consequence, the relative signal $SIG_{rel,x}$ for thin films can be obtained by two different acquisition strategies. One approach is the measurement of the full spectrum $\int S_{v=x}(\lambda, T)d\lambda$ of a single vibrational state. As described above, raw signals are compared from a crystal partially consisting of clean Au(111) and partially of a homogeneous deposited film. Because the acquisition of a spectrum takes several minutes that is a rather time-consuming way to measure many data points of different film thickness. As an alternative, we tested if it is sufficient to focus on the REMPI intensity of a single rotational state. Using a constant REMPI wavelength, we assumed that different surfaces can easily be compared by scanning the molecular beam along different surface positions with known film thickness. With a wedge grown on the surface (see Fig. S3), many data points can be acquired in a shorter time span.

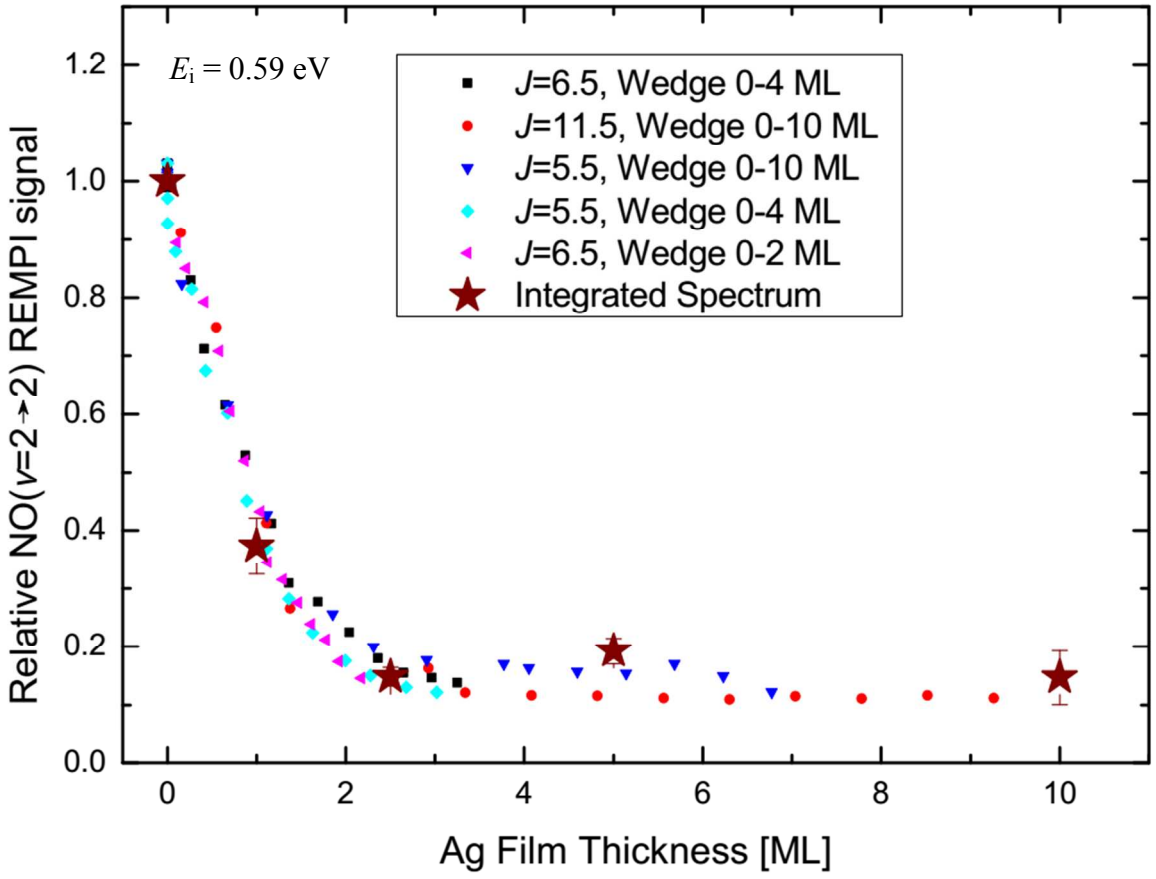

Fig. S5: State-selective NO(v = 2→2) signal at different film thicknesses. One strategy focuses on the intensity measured from a constant rotational state along a silver wedge grown on the Au(111) sample. The other approaches compares the integrated vibrational spectrum obtained from a sample consisting to 50% of a homogeneously coated silver film. All signals are referenced to the one obtained after scattering from clean Au(111). Both acquisition strategies deliver the same result.

Both acquisition strategies are compared in Fig. S5. The plot shows the relative NO(v = 2 → 2) signal in arbitrary units with the signal obtained from clean Au(111) set as a reference. We see that both approaches lead to the same result helping us to employ a more time-efficient measurement technique.

3. Angular Distributions of NO(v = 2 → 2,1)

Fig. S6 shows the angular distributions for both experimentally observed vibrational channels. In all cases, only negligible influence of the surface and narrow distributions are observed peaking close to the incident angle (black arrow). When fitting the data points by a $\cos^n$-shaped function, high values of the exponent n>>1 are obtained. The mechanism can therefore be described as direct scattering. In contrast, an exponent of n=1 would have been expected for a trapping-desorption mechanism.

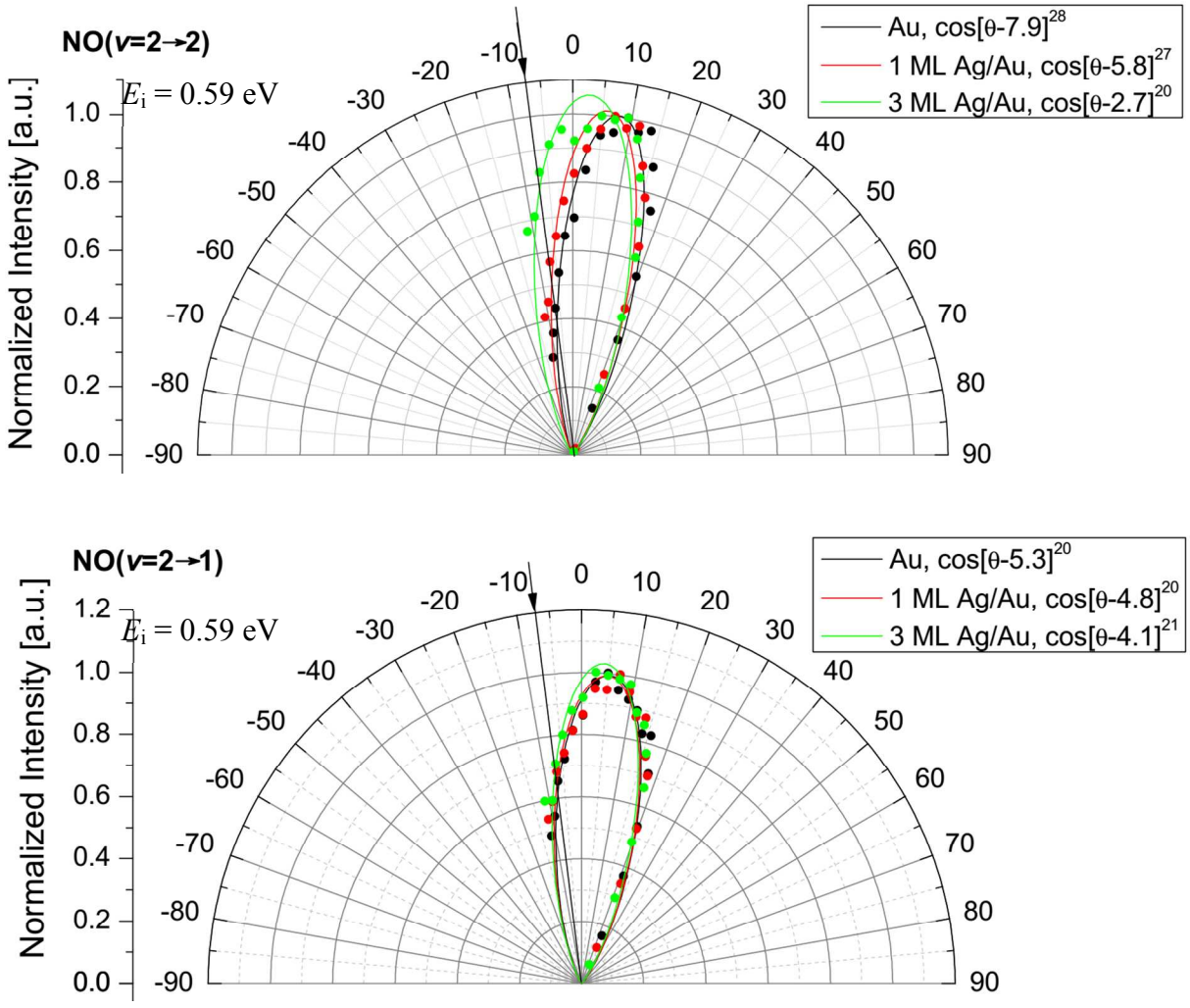

Fig. S6: Angular Distributions for NO(v = 2→2,1) with increasing thickness for E_i = 0.59 eV.

4. Molecular Vibrational Relaxation within the Newns Model

The model introduced by Newns (Ref: Newns, D. M., Electron-Hole Pair Mechanism for Excitation of Intramolecular Vibrations in Molecule-Surface Scattering. *Surf. Sci.* **1986**, *171*, 600-14.) provided the first theoretical approach to describe nonadiabatic vibrational energy transfer at a metal surface. It was employed for the special case of vibrational excitation of NO($v = 0$) into the first excited vibrational state ($v = 1$) after scattering from a hot Ag(111) surface as experimentally observed by Rettner *et al.* (Rettner, C.T.; Fabre, F.; Kimman, J., Auerbach, D.J., Observation of Direct Vibrational Excitation in Gas-Surface Collisions: NO on Ag(111), *Phys. Rev. Lett.* **1986**, *55*, 1904-7). With reasonable assumptions, the model reproduced the dependence of the excitation probability $\bar{n}$ on the normal translational incidence energy $E_\perp$.

Both molecular vibrational excitation and relaxation have been described by the same mechanism, a coupling between the vibrational degrees of freedom with the electron-hole pairs (EHPs) of the surface. Accordingly, we assumed that the Newns theory can be applied to predict the relaxation probability of NO($v = 2$) at ultra-thin metallic films in a similar manner. The model depends on several parameters but the work function ϕ and the electron affinity A_{NO} only enter through their difference.

Equation (43) in Newns' publication was used to calculate the relaxation probability as a function of $-\epsilon_\infty = A_{NO} - \phi$ in the original notation. We assume that this parameter corresponds to $\Delta \equiv VEBE_{r_>} - \phi$ in the case of vibrational relaxation replacing A_{NO} by $VEBE_{r_>}$, the molecule's vertical electron binding energy at the outer turning point. Other parameters were chosen as in Newns' calculation for NO/Ag(111).

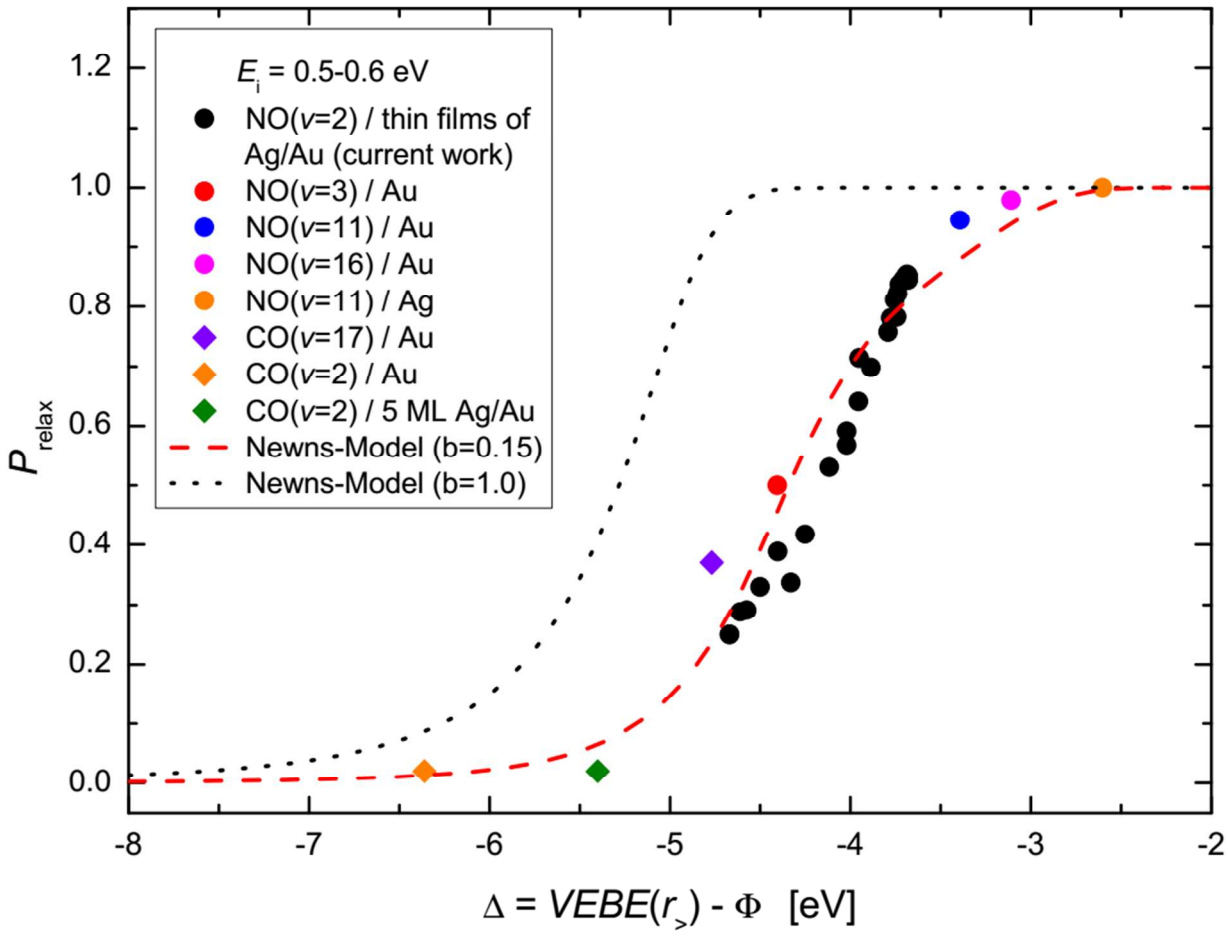

Fig. S7: Modeling relaxation probability as a function of Δ. Depending on the chosen Bose factor, the calculation by the Newns model is depicted (red dashed line and black dotted line). Experimental data for a number of different molecules-surface systems (E_i = 0.5-0.6 eV) are shown as well. The Newns model predicts the trend of increasing relaxation probability with Δ.

Two adjustments had to be made in comparison to the original calculation by Newns. First, as it is physically not possible for relaxation probabilities to exceed values above unity, the obtained values were restricted to <1 using a *tanh*-shaped saturation function. The resulting curve does not critically depend on the choice of the saturation function. This adjustment is required to make the model behave physically correct. Second, an assumption had to be taken for the Bose factor (notation in the original paper: $b(\omega_0)$). One limiting factor for NO excitation is the density of

excited EHPs at the surface that transfer energy to the molecule. In contrast, during relaxation of NO(v = 2), vibrational energy is transferred to non-excited EHPs. At room temperature, due to the high density of such states, that factor is expected to be approximately equal to 1. While the qualitative shape of the calculation is independent of the Bose factor, we found that for a quantitative agreement a Bose factor of 0.15 is needed. Obviously, this second adjustment is to some degree arbitrary and its physical interpretation is not perfectly clear.

For both cases, the results are plotted in Fig. S7. The calculated functions exhibit a shape very similar to the experimental data for different cases of molecular relaxation. Our main result is that the Newns model used for nonadiabatic vibrational excitation predicts qualitatively the experimentally observed trend of increasing relaxation probability with Δ.